Soil Dynamics and Earthquake Engineering 127 (2019) 105839

Contents lists available at ScienceDirect

Soil Dynamics and Earthquake Engineering

journal homepage: www.elsevier.com/locate/soildyn

Numerical modeling of liquefaction and its impact on anchor piles for floating offshore structures

Pourya Kazemi Esfeh[a], Amir M. Kaynia[b,c,*]

[a] Department of Civil, Chemical, Environmental, and Materials Engineering, University of Bologna (UNIBO), Italy
[b] Norwegian Geotechnical Institute (NGI), Norway
[c] Norwegian University of Science and Technology (NTNU), Trondheim, Norway

ARTICLE INFO

Keywords:
Liquefaction
Anchor pile
Seismic analysis
SANISAND constitutive model
Offshore foundations
Offshore wind

ABSTRACT

Anchor piles and suction anchors have been used for anchoring different types of offshore structure in the past four decades. The recent growing interest and demand for wind energy has motivated the industry to evaluate the use of Offshore Wind Turbines (OWT) in deep waters for which floating wind turbine is a good alternative to bottom-fixed solutions particularly in seismic regions with possibility of soil liquefaction. Extensive research has been carried out to assess the consequences of soil liquefaction for buildings and onshore structures; however, this phenomenon has not been sufficiently studied for offshore foundations. This paper aims at investigating the use of advanced liquefaction modeling in assessment of the performance of anchor piles for offshore facilities and in particular floating offshore wind turbines. The software FLAC3D is used to carry out the nonlinear dynamic analyses using SANISAND constitutive model for saturated sand. The analyses indicate that SANISAND model is capable of correctly simulating the excess pore water pressure in the free-field as observed in centrifuge tests. Pore pressure build-up due to earthquake shaking together with earthquake-induced displacements are computed at various points in the soil medium containing an anchor pile in different scenarios. The numerical results indicate that anchor piles may experience permanent lateral displacements and tilt due to the combined action of static mooring load and earthquake shaking leading to soil liquefaction.

1. Introduction

Anchor piles and suction anchors have been used for mooring different types of offshore facilities for more than several decades. The recent growing interest and demand for wind energy has motivated the industry to evaluate the use of Offshore Wind Turbines (OWT) in deep waters for which flowing wind turbine (Fig. 1a) is a good alternative to bottom-fixed solutions (Fig. 1b). Moreover, anchor piles are attractive in seismic regions, especially in areas with possibility of soil liquefaction. The first large-capacity (3 MW) floating OWT was installed offshore Norway in the North Sea in September 2009. After several years of attempts, the first commercial floating offshore wind farm consisting of 5 Hywind turbines anchored by suction piles was installed offshore Scotland in 2015. Following this success, Japan deployed its first floating OWT supported by suction anchors near Fukue Island in 2016. Offshore wind energy keeps on growing significantly, with floating OWT capacity expected to increase from 36 MW today to 4–5 GW in 2030 [1].

The main concern in the design of offshore foundations in Northern Europe has been environmental loads, whereas in seismically active areas (e.g. East Asia and Southern Europe) the earthquake loading and liquefaction in loose silt and sand could play a governing role on stability and reliability of these structures [2]. Although there has been a consensus within the engineering community that moderate earthquake

* Corresponding author. Norwegian Geotechnical Institute (NGI), Oslo, Norway.
E-mail addresses: pooria.kazemi@studio.unibo.it (P.K. Esfeh), amir.m.kaynia@ngi.no (A.M. Kaynia).

https://doi.org/10.1016/j.soildyn.2019.105839
Received 2 May 2019; Received in revised form 16 July 2019; Accepted 28 August 2019

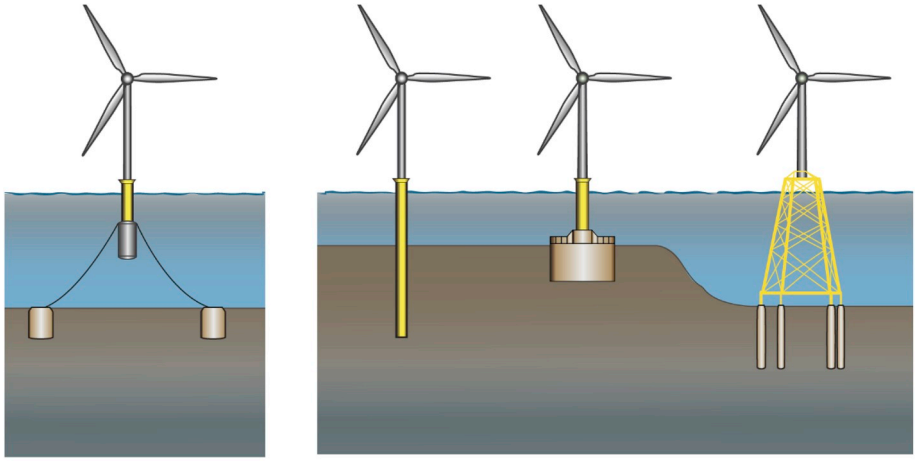

Fig. 1. Foundations for offshore wind turbines: a) Floating wind turbines, b) Types of bottom-fixed offshore wind turbines.

Table 1
Summary of soil sample properties used in triaxial tests [27].

Property	Relative density D_r (%)		
	40	60	90
Void ratio, e	0.69–0.7	0.64–0.65	0.55–0.56
Hydraulic conductivity, k (m/s)	1.41×10^{-4}	1.36×10^{-4}	1.19×10^{-4}
Peak friction angle, φ_p (degrees)	32–32.5	34.8–36.5	41.5–42.1
Phase transformation angle φ_{PT} (degrees)	25.1–31.2	24.5–30	22.2–28.5

Table 2
Summary of initial soil conditions in the centrifuge experiment [30].

Thickness/D_r/Layer	e	γ_{sat} (kN/m^3)	k (m/s)
2 m/90%/Monterey	0.57	19.8	5.30×10^{-4}
6 m/40%/Ottawa sand F65	0.7	19.1	1.41×10^{-4}
10 m/90%/Ottawa sand F65	0.56	19.9	1.19×10^{-4}

loading is not of highest significance in design of OWTs, the growing trend in offshore wind turbine construction in highly seismic areas has necessitated a more critical evaluation of this matter. Recent studies on the influence of a combination of wind and earthquake loads on OWTs [3–5] have highlighted the significance of seismic loading in design of these structures. In particular, liquefaction has a major impact on OWT foundations. While most foundation types, such as monopiles, skirted caissons and piles for jacketed structures (Fig. 1b) carry large gravity loads leading to excessive permanent deformations during liquefaction, anchors have the role of stabilizing the structures during extreme environmental loading; therefore, their movements during an earthquake

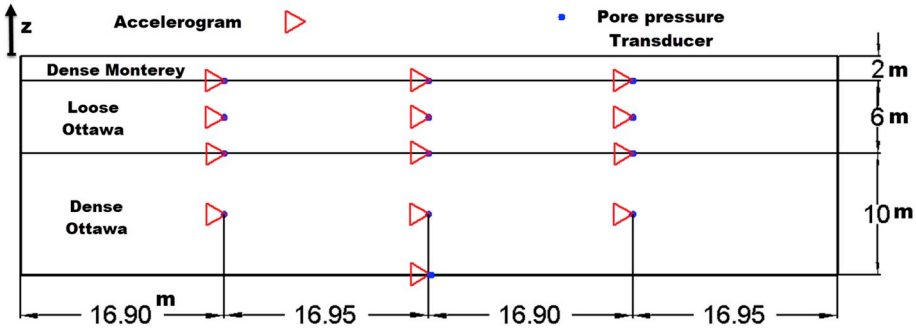

Fig. 2. Layout of centrifuge experiment [30]. Dimensions are in prototype scale for 70 g centrifugal acceleration.

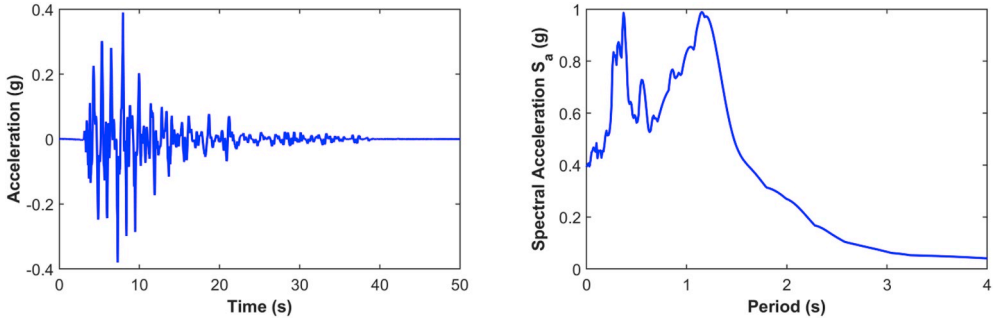

Fig. 3. Acceleration time history and spectral acceleration (5% damping) of Kobe-L earthquake applied at base of container [30].

Table 3
Parameters of SANISAND constitutive model calibrated for Ottawa sand F65 [27].

Property	Value
Elastic material constant, G_0	125
Poisson's ratio, υ	0.05
Critical state stress ratio, M	1.26
Ratio of critical-state stress ratio in extension and compression, c	0.735
State line constant, λ_c	0.0287
Void ratio at p = 0, e_0	0.78
State line constant, ξ	0.7
Yield surface constant, m	0.02
h_0	5
c_h	0.968
n^b	0.6
A_0	0.5
n^d	0.5
z_{max}	11
c_z	500
$\bar{e}^p_{eq}$ (%)	0.01
n	1

might not pose a substantial threat to the performance of the structure. It is only in taut mooring systems that liquefaction could result in pulling off the anchors with major design consequences. In any case, it is essential to be able to compute the response of anchors under the combined actions of horizontal mooring forces and liquefaction during earthquake shaking.

Over the past few decades, laboratory tests (e.g. Refs. [6,7]), CPT and SPT based liquefaction triggering procedures (e.g. Refs. [8–10]), and numerical modeling (e.g. Refs. [11–14]) have been conducted to predict the liquefaction potential and the possible consequences of liquefaction on structures. These studies have covered, among others, estimation of the number of cycles to initiation of liquefaction, pore water pressure generation, liquefaction-induced displacements and site response during earthquake.

Despite considerable research on liquefaction, the number of studies reported on the performance of foundations under liquefaction is relatively limited. The nonlinear p-y spring models are among popular approaches for analyzing OWT foundations on mono-piles. These models can be extended to earthquake analyses by defining appropriate hysteretic behavior for the springs (e.g. Ref. [15]) and using additional elements for representing the far-field during earthquake loading [16]. However, these models are not capable of simulating buildup of the pore water pressure and its impact on the foundation response. Hence, finite element/finite difference (FE/FD) codes have been used for this purpose (e.g. Refs. [17,18]). The inadequacy of classical constitutive models to realistically simulate the pore pressure response under cyclic loading conditions necessitates use of more advanced constitutive models in numerical codes. Over the past few decades, tremendous efforts have been made to develop constitutive models capable of predicting the seismic response, shear/volumetric strain accumulation and pore pressure generation of soil structures under seismic loading (e.g. Refs. [19–22]). In this paper, the simple anisotropic constitutive model for sand (SANISAND) developed by Dafalias and Manzari [20] and implemented in 3D software FLAC3D has been utilized for fully-coupled dynamic analyses. The capabilities of advanced constitutive models to capture the soil response under cyclic loading have often been evaluated based on the results of element-level or centrifuge tests (e.g. Refs. [23–27]).

Ziotopoulou [25] validated the constitutive model PM4Sand [22] using the finite difference program FLAC with the LEAP centrifuge tests [28]. The results of this study have indicated that PM4Sand model is capable of simulating the response of liquefiable sloping ground. Ramirez et al. [27] carried out a series of centrifuge tests and used the data for an evaluation of different numerical tools. These authors studied the performance of SANISAND and PDMY02 [29] constitutive models using a series of monotonic and cyclic (drained and undrained) triaxial tests in two phases. During the first phase, referred to as calibration C, the model parameters were determined so that the soil behavior was consistent, at the element level, with the results of triaxial tests. Subsequently, they used the results of a series of centrifuge tests of a liquefiable sand with base shaking (site response analyses) to further refine

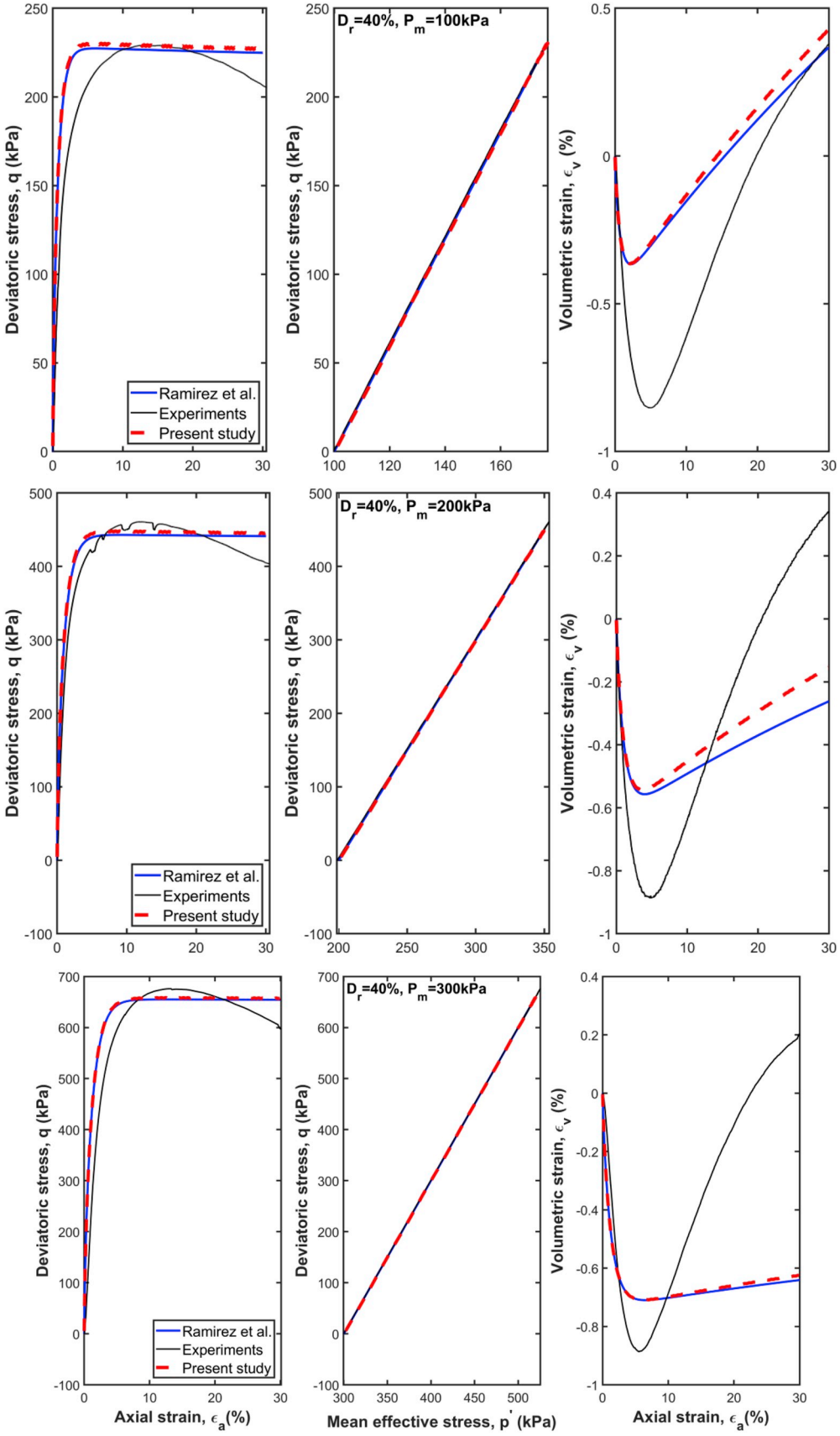

Fig. 4. Comparison between numerical and experimental results for monotonic drained triaxial tests on loose Ottawa sand with D_r = 40%.

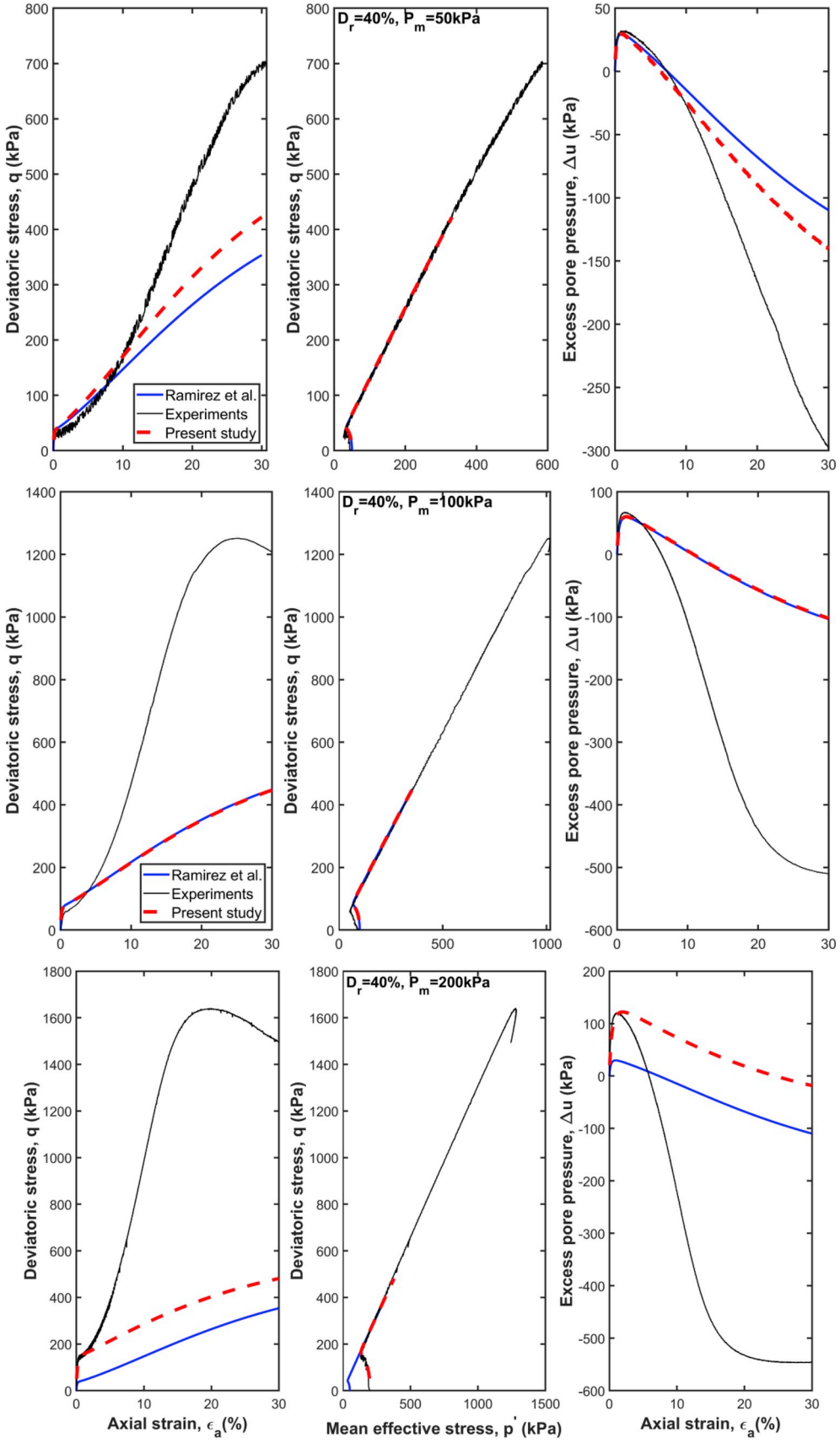

Fig. 5. Comparison between numerical and experimental results for monotonic undrained triaxial tests on loose Ottawa sand with D_r = 40%.

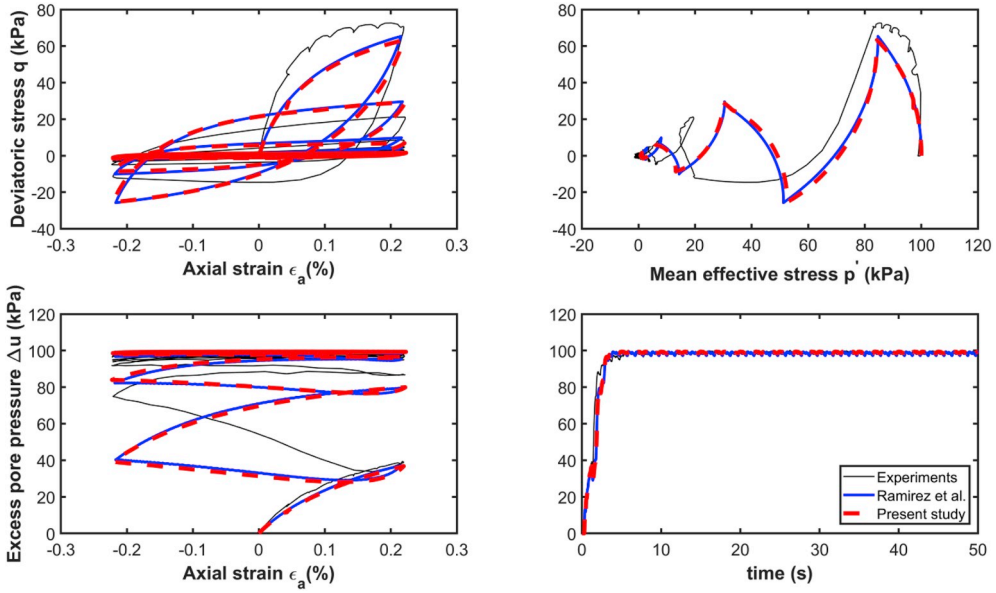

Fig. 6. Comparison between numerical and experimental results for cyclic undrained triaxial tests on Ottawa sand with D_r = 40%.

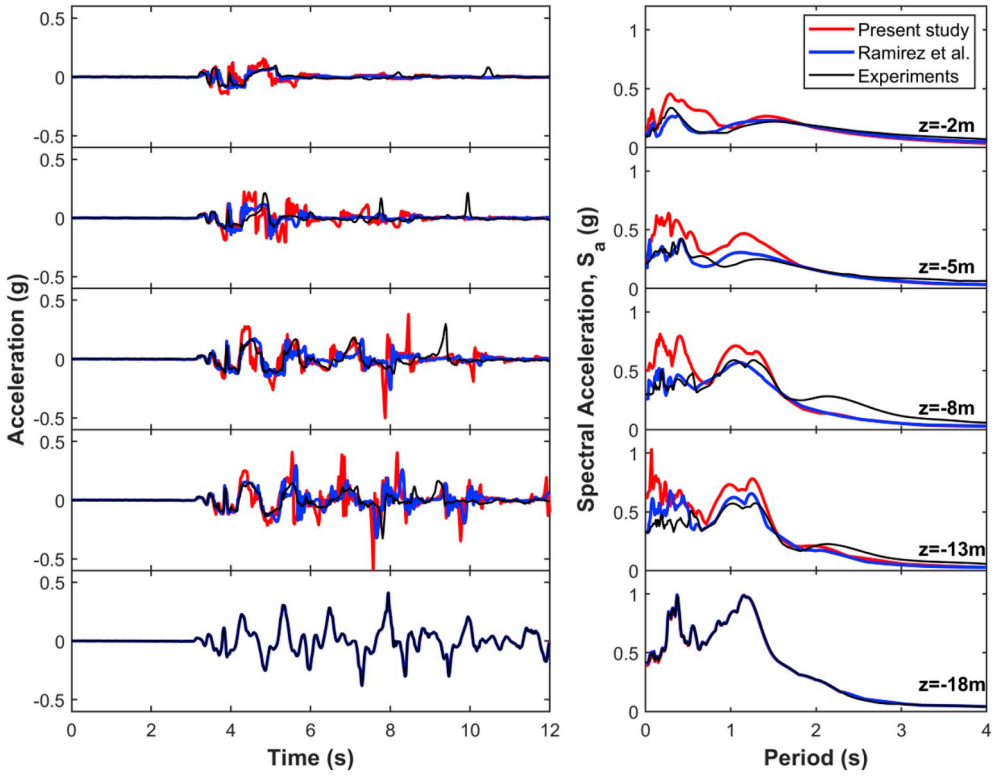

Fig. 7. Comparison between numerically calculated and experimentally measured acceleration time histories and corresponding response spectra in centrifuge test.

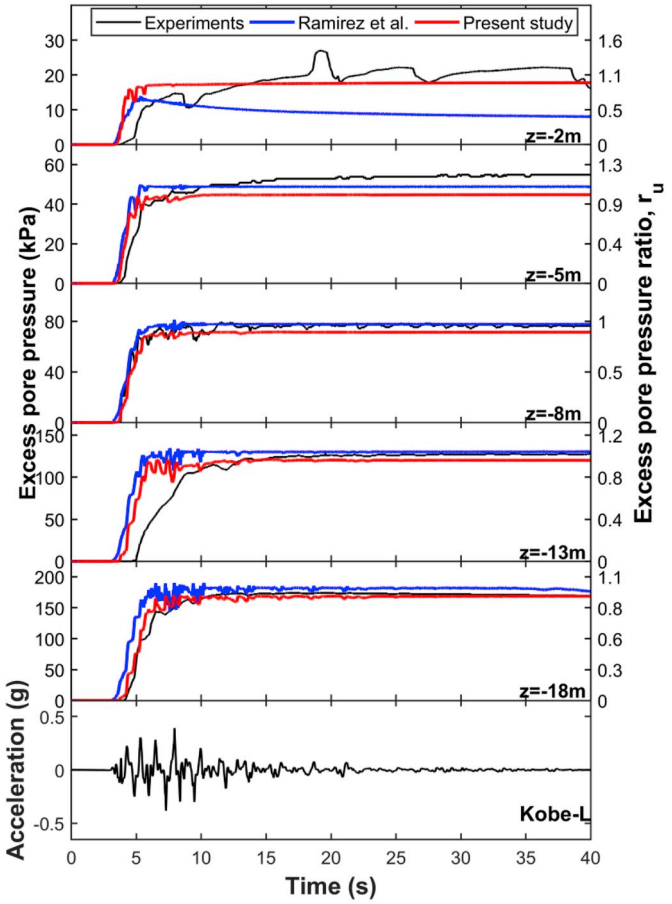

Fig. 8. Comparison of numerically calculated and experimentally measured excess pore water pressures in centrifuge test.

the parameters, referred to as calibration C1.

This paper aims at numerically investigating the effect of liquefaction on anchor piles for offshore structures and offshore wind turbines subjected to a combination of mooring load and earthquake shaking. To this end, the finite difference software FLAC3D was employed to carry out the fully-coupled dynamic analyses. The constitutive model SANISAND with the same model parameters proposed by Ramirez et al. [27] was used in the analyses.

In order to gain insight into the performance of anchor piles and suction anchors during liquefaction, several scenarios of environmental loading and soil/pile characteristics were considered in this study.

2. Model verification

The parameters of SANISAND model were verified using a series of strain-controlled monotonic and cyclic tests using FLAC and the site response analyses in the centrifuge experiment [27]. In the present study, FLAC3D was used to confirm the model parameters using a series of monotonic and cyclic (drained and undrained) tests. The intention was to use the same soil and model parameters in the numerical model of the soil with the anchor pile.

2.1. Triaxial tests

The triaxial compression tests were performed on Ottawa sand F65 by Ramirez et al. [27]. Ottawa sand F65 (characterized by $D_{50}=0.15$ mm, $C_u=1.45$, $e_{min}=0.53$, $e_{max}=0.82$) is classified as an SP soil based on the Unified Soil Classification System (USCS). Since the layered soil in the centrifuge test contains three layers with various relative densities, the soil samples were prepared at three relative densities ($D_r=40\%$, 60% and 90%) to accurately represent the fabric of the soil in the centrifuge experiment. The specimens were isotropically consolidated to three levels of confining pressures (100, 200 and 300 kPa) for drained monotonic compression tests. For undrained monotonic compression tests, the soil samples were prepared at the same levels of relative densities and were consolidated to three confining pressures of 50,100 and 200 kPa. All the samples for the cyclic undrained test were isotropically consolidated to the confining pressure of 100 kPa. Strain-controlled cyclic axial load was applied to the model with a frequency of 1 Hz and with amplitudes ranging from 0.042% to 0.44%. Table 1 lists the soil parameters resulting from the triaxial tests.

2.2. Centrifuge experiment

In this study, the centrifuge experiment with free-field conditions (i.e. no structure) in a flexible shear beam (FSB) container conducted by Kirkwood and Dashti [30] was used for model calibration (Fig. 2). The tests were performed under a centrifugal acceleration of 70 g in the 5.5-m radius beam centrifuge at the University of Colorado, Boulder [30]. The total height of the soil was 18 m in prototype scale including 10 m of dense Ottawa sand at the bottom, 6 m of loose Ottawa sand (liquefiable layer) in the middle, and 2 m of dense Monterey sand on top. The bottom Ottawa sand layer was dry-pluviated at relative density D_r = 90%, the liquefiable layer was formed of the same Ottawa sand with D_r = 40%, and the top Monterey sand layer, characterized by D_{50} = 0.40 mm, C_u = 1.3, e_{min} = 0.54, e_{max} = 0.84 [30], was prepared at D_r = 90%. Table 2 summarizes the geotechnical characteristics of the soil layers.

The pore pressure transducers, accelerometers and vertical LDVTs were positioned at several depths in three different arrays (left, center and right) far from the boundaries of the container to measure excess pore pressures, accelerations and vertical displacements during the shaking. The model was spun with a centrifugal acceleration of 70 g.

A series of the horizontal acceleration time series were applied to the base of the container while spinning. The scaled version of the north-south fault normal horizontal component of the Kobe, Japan earthquake recorded at Takatori station (Kobe-L earthquake record) was used in this study. Kobe-L earthquake has PGA = 0.41 g, significant duration $D_{5\text{-}95\%}$ = 12 s, and mean period T_m = 0.87 s. Fig. 3 presents the time history and acceleration response spectrum S_a (damping 5%) of Kobe-L earthquake record applied at the base of the container.

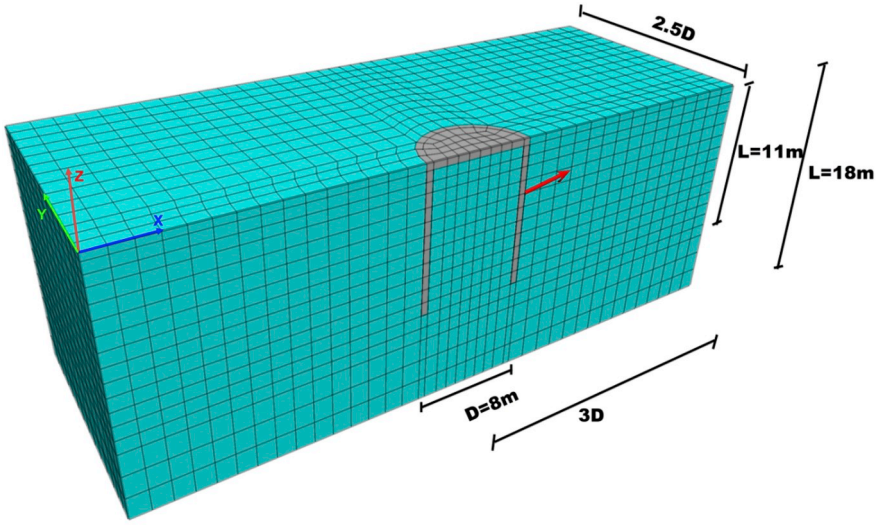

a)

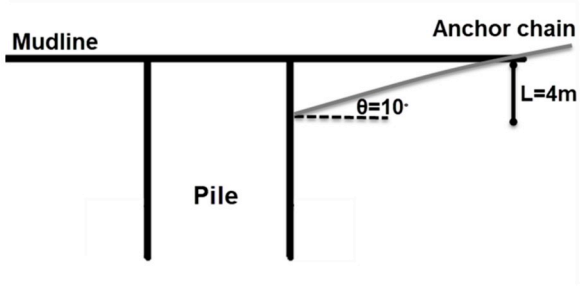

b)

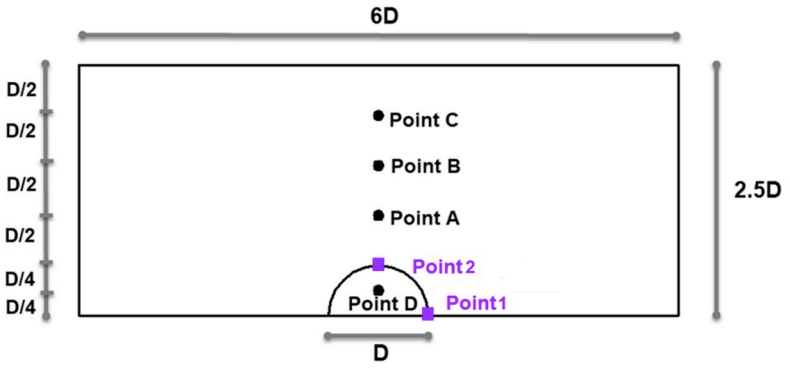

c)

Fig. 9. Anchor pile sketches: a) finite difference model, b) longitudinal section, c) plan view of monitoring points for response.

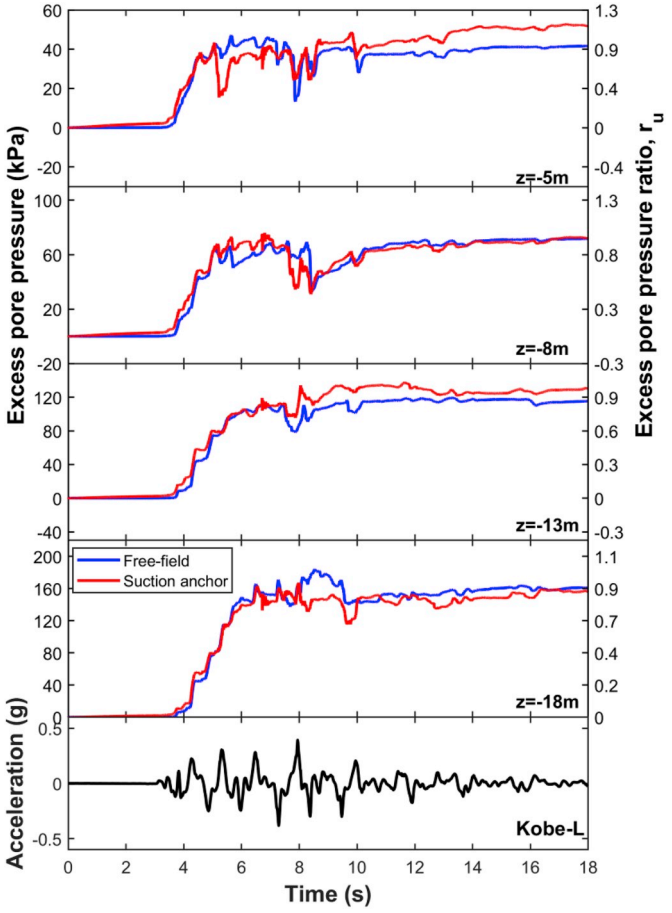

Fig. 10. Excess pore water pressure at point A in Case 1 and comparison with free-field pore pressures.

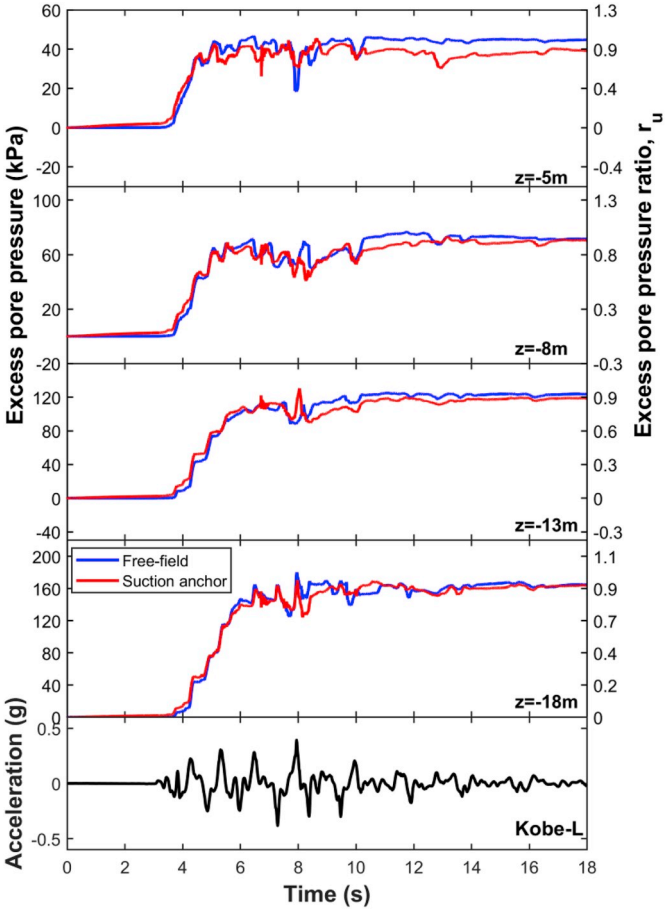

Fig. 11. Excess pore pressure at point B in Case 1 and comparison with free-field pore pressures.

2.3. Numerical analyses

The finite difference software FLAC3D was adopted for the dynamic analyses in the present study. FLAC3D is capable of performing coupled fluid mechanical analysis following the formulation of poro-elasticity proposed by Biot [31] and later adopted by Detournay and Cheng [32] for the FLAC platform. The bulk modulus and density of water were set, respectively, equal to 2 GPa and 1000 kg/m^3 in the simulations.

The SANISAND constitutive model was selected for simulating the nonlinear behavior of the sandy soil. SANISAND is the term referred to a group of anisotropic constitutive models developed to realistically simulate the behavior of sands under monotonic and cyclic loading in drained and undrained conditions. This constitutive model, first proposed by Manzari and Dafalias [33], is based on the two-surface formulation of plasticity and state parameter concept within the framework of critical state soil mechanics. The SANISAND class comprises various extensions where each of them was modified for different aspects of soil behavior. The SANISAND model extended by Dafalias and Manzari [20] to account for fabric change effect was considered in this study.

The elastic part of the SANISAND model is characterized by the small-strain shear and bulk moduli G and K that depend on the mean effective stress. The hardening behavior of the soil is governed by the plastic modulus defined by h_0, c_h, and n^b in deviatoric space. The plastic modulus changes based on the bounding condition represented by the distance between the actual stress point and its corresponding stress point on the bounding surface. The plastic deformations are restricted by bounding surface to occur merely for the stress ratios on or within the bounding surface. The plastic volumetric strains are coupled with the plastic deviatoric strains based on Rowe's dilatancy rule through parameters A_0 and n^d. The size of the yield surface cone is specified by the parameter m, and the critical-state surface is determined by the parameters M and c in the q-p' space (λ_c, e_0, and ξ in the p-e' space). The effect of fabric changes on dilation-contraction behavior of the soil under cyclic loading is controlled by the parameters z_{max} and c_z. The parameters $\bar{e}^p_{eq}$ and n account for overshooting response upon small unloading-loading scenarios occurring in bounding surface models. Table 3 lists the model parameters as calibrated by Ramirez et al. [27].

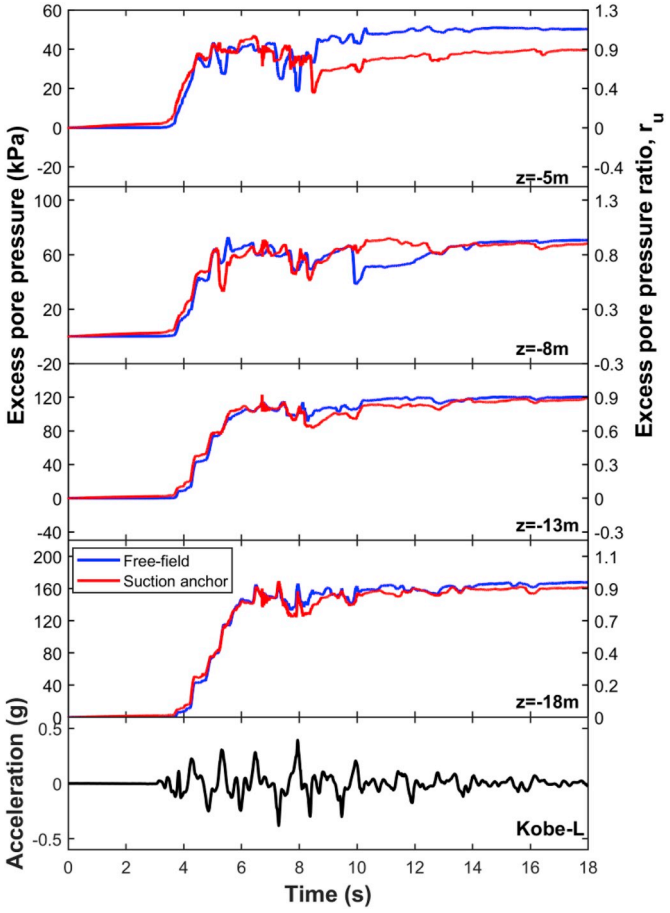

Fig. 12. Excess pore water pressure at point C in Case 1 and comparison with free-field pore pressures.

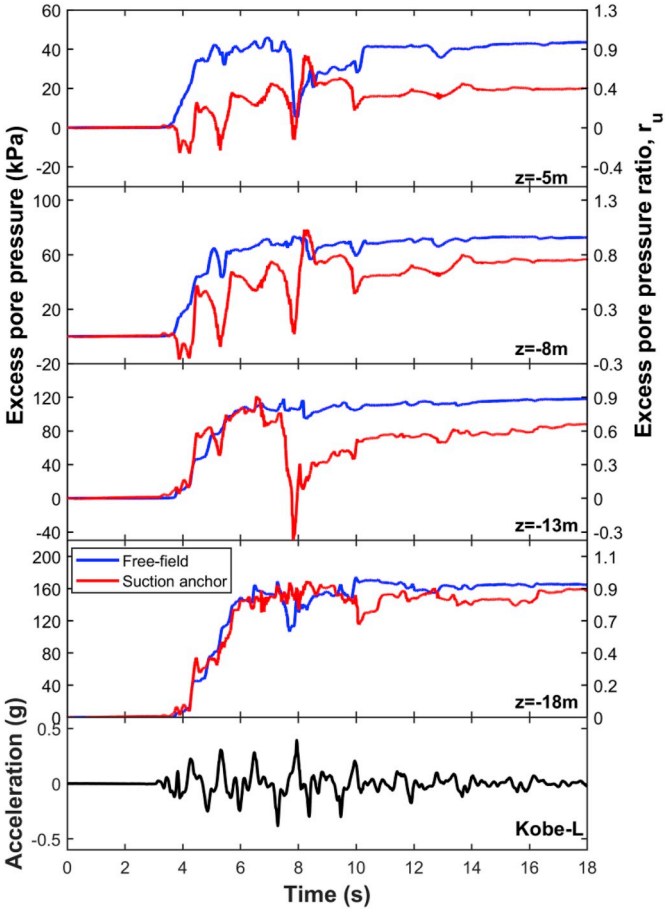

Fig. 13. Excess pore water pressure at point D in Case 1 and comparison with free-field pore pressures.

2.4. Soil parameter calibration

Ramirez et al. [27] first calibrated the model parameters with a series of drained/undrained monotonic and cyclic triaxial tests referred to calibration C. Next, they adjusted the model parameters to better reproduce the results of centrifuge site response experiments (referred to as calibration C1). In the present study, only the model parameters after calibration C1 were used (Table 3). The following presents the results of some of the verifications performed in this study.

2.4.1. Comparisons of element-level numerical and experimental results

Figs. 4 and 5 compare the results of monotonic triaxial tests with the numerically simulated values for the loose sand. The comparisons for the dense sand are presented in Appendix A. It can be observed that the initial stiffness and peak deviatoric stress are estimated well by SANISAND model for loose Ottawa sand under the considered range of confining pressures (equally good match was obtained for dense Ottawa sand). The softening behavior of sand (i.e., the reduction in deviatoric stress post the peak) is also properly captured for all confining pressures and soil conditions, especially for dense sand. The stress-strain responses predicted in this study using FLAC3D are very similar to those estimated in Ref. [27] except that FLAC3D evaluates slightly higher volumetric strains for the loose sand. In general, predicting the stress-strain response of sand and excess pore water pressure under undrained condition is a more laborious task. The figures demonstrate that FLAC3D has estimated the stress-strain responses and excess pore pressures for the undrained tests more accurately than FLAC [27].

The numerical and experimental results for cyclic undrained tests on loose sand are compared in Fig. 6, and the results for dense sand are presented in Appendix A. As demonstrated in these figures, the stress-strain response and excess pore pressure derived from the numerical simulations are reasonably consistent with those measured in triaxial tests for both loose and dense sandy soils indicating that SANISAND is capable of satisfactorily capturing the cyclic behavior of soil at element level. A closer look at Fig. 6 confirms that the results of the cyclic undrained triaxial simulations in this research are close to the results of Ramirez et al. [27] using FLAC.

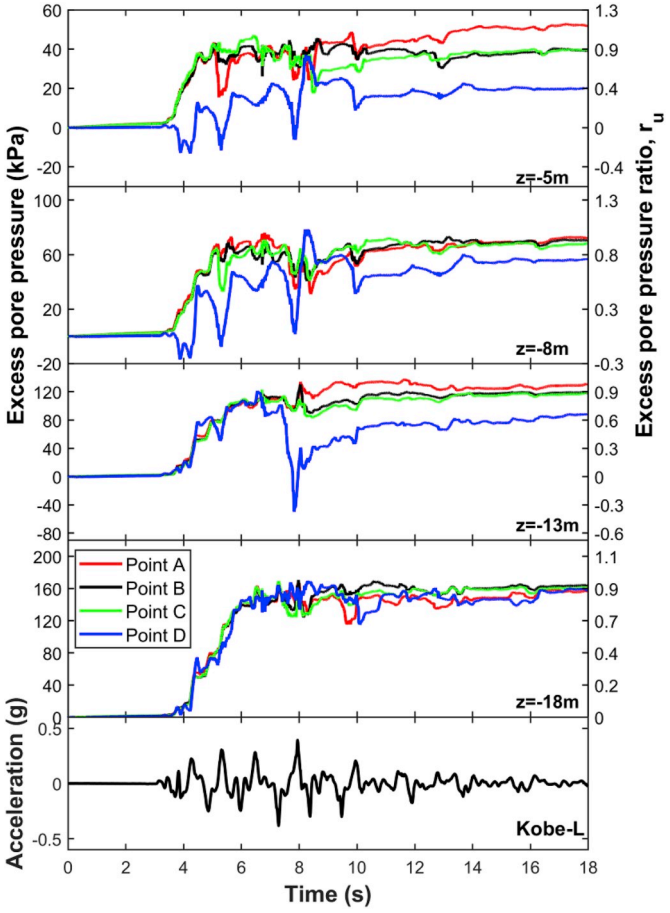

Fig. 14. Excess pore water pressures at monitoring points in Case 1.

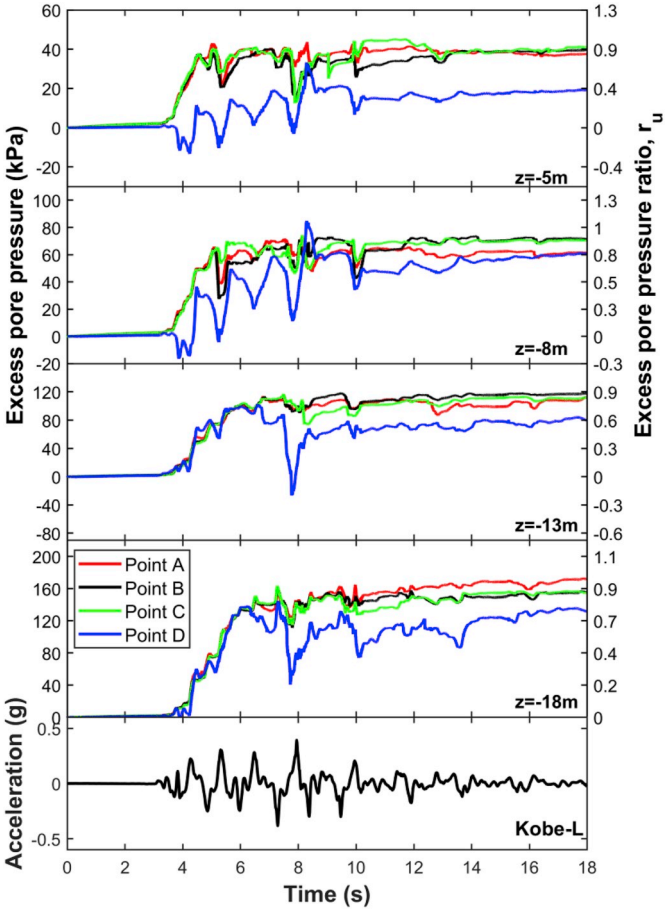

Fig. 15. Excess pore water pressures at monitoring points in Case 2.

2.5. Simulations of centrifuge experiment

The elastoplastic site response of the soil in the centrifuge experiment was evaluated using a soil column in FLAC3D with tied boundary conditions. The SANISAND constitutive model with the parameters in Table 3 was assigned to the soil layers. The minimum Rayleigh damping ratio $\xi_{min} = 2.24\%$ and a center frequency of 5.5 Hz were used in the simulations.

The acceleration time history in Fig. 3 was applied to the rigid base of the model in FLAC3D. Fig. 7 displays the computed acceleration time histories at a number of points along the soil profile together with the corresponding response spectra for 5% damping. As the figure shows, the accelerations at different depths are consistently reproduced during the first cycles of shaking. Moreover the response spectra look fairly similar to those of the measured motions although some discrepancies can be observed at higher frequencies. The figure also includes the results computed in Ref. [27]. There is generally good agreement between the results of the two studies. Fig. 8 displays the time histories of the simulated excess pore water pressures at the same depths together with the experimental data and the results from Ref. [27]. The excess pore pressure is presented in terms of excess pore pressure ratios, $r_u = \Delta u/\sigma'_{v0}$ (where σ'_{v0} is the initial effective vertical stress. $r_u > 0.95$ is recognized as liquefaction criterion).

3. Numerical modeling of anchor pile

The constitutive model and the finite difference model described in the preceding section were used for assessment of the earthquake response of a realistic anchor pile in a liquefiable soil due to earthquake shaking. The calibrated quadrilateral elements in FLAC3D were used for modeling both the soil and the anchor pile. Due to symmetry, half of the anchor was modeled. Fig. 9a displays the FD mesh and model dimensions. The tied boundary option was found to produce the best results and minimization of boundary effects. The sizes of the soil zones were set up based on the requirement for wavelength corresponding to the maximum frequency content of Kobe-L earthquake record applied at the base of the model.

The anchor pile considered in this study is representative of anchors

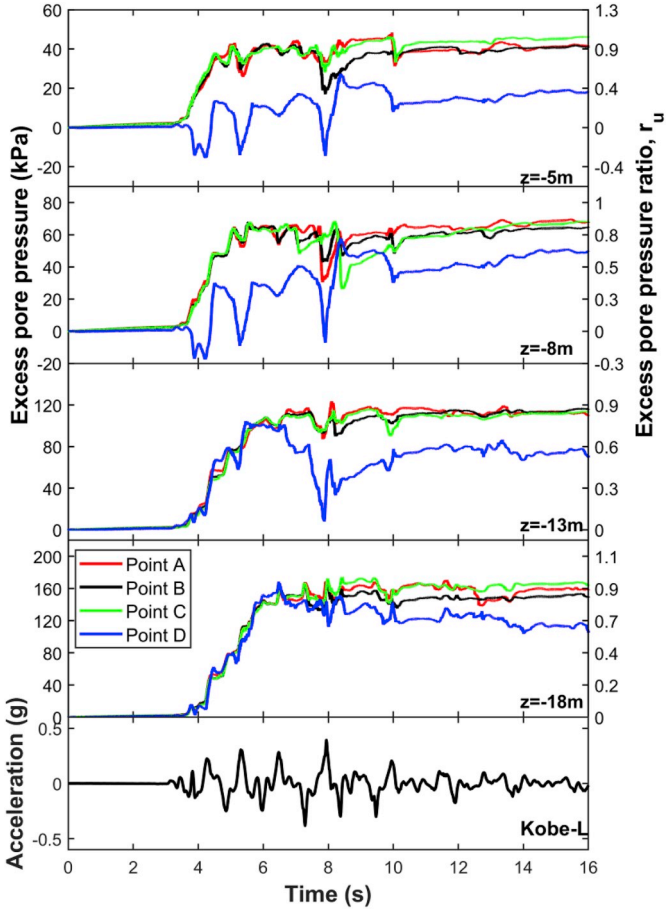

Fig. 16. Excess pore water pressures at monitoring points in Case 3.

for a floating OWT (with a typical power ~8 MW). The dimensions are: Diameter D = 8 m, Length L = 11 m and Wall thickness t = 4 cm. The linear elastic model with Young's modulus E_{steel} = 210 GPa and mass density ρ_{steel} = 7800 kg/m^3 was assigned to the steel anchor pile. To avoid large aspect ratios of elements in the pile, the thickness of the skirt was increased to 50 cm and the elastic modulus and mass density were correspondingly reduced. The elastic modulus E_{eq} and unit mass ρ_{eq} of the modified pile were established in a way to maintain the same total mass and the same bending rigidity of the real pile using the equations $E_{eq}\ I_{eq} = E_{pile}\ I_{pile}$ and $\rho_{eq}\ A_{eq} = \rho_{pile}\ A_{pile} + \rho_{soil}\ (A_{eq} - A_{pile})$, where E_{pile} and I_{pile} are the elastic modulus and moment of inertia of the anchor pile section, respectively, I_{eq} is the moment of inertia of the modified (equivalent) pile; similarly ρ_{pile} and A_{pile} are the unit mass and cross sectional area of the anchor pile, A_{eq} is the cross sectional area of the modified pile, and ρ_{soil} and is the unit mass of the soil. Use of the parameters of the soil and anchor pile resulted in E_{eq} = 19 GPa and ρ_{eq} = 2450 kg/m^3.

Pile-soil interfaces were created on zone faces around the anchor pile to approximately represent the contact conditions at the soil-pile interface. Interfaces available in FLAC3D use a constitutive model defined by a linear Coulomb shear-strength model that limits the shear force acting at an interface node together with normal and shear stiffnesses at the contact. The interface friction angle was considered as 80% of the peak friction angle of loose Ottawa sand (i.e. $\varphi_p \sim 33^\circ$, see Table 1) to take into account the pile's reduced skin resistance at the interface. The normal and shear stiffnesses of the interface (k_n and k_s) were set to ten times the stiffness of the neighboring zone.

The load at the pad-eye of the anchor pile was taken less than the design (maximum) environmental load on the mooring line (Fig. 9b). The load was applied to the anchor pile as a concentrated static load with an angle θ = 10 deg. to the horizontal at the pad-eye located at a depth of 4 m from the surface (Fig. 9b). The angle of the load is determined in practice by an inverse catenary analysis of the mooring chain. However, experience has shown that this angle might reduce with time; especially, during liquefaction, the chain is expected to sink more into the soil thereby reducing the load angle. The above angle was selected by a consideration of these concepts, and it represents a more critical condition compared to a case of larger load angle.

The anchor's ultimate resistance (capacity) was estimated by applying a constant velocity in the load's direction until failure was reached (i.e., where an apparent flattening in the load-displacement response was observed). The anchor's ultimate resistance was computed approximately equal to 6 MN. The flow mode was on in establishing the initial pore pressure distribution in the free-field. Afterward, the flow mode was turned off during application of the mooring load and earthquake shaking for proper generation of pore water pressure. The anchor pile was considered impermeable in the analyses. The analyses were carried out using the small-strain solution to reduce the run time and to avoid possible numerical instabilities. Based on the computed maximum shear strains (about 15%), this assumption is believed not to have significantly affected the results.

4. Analysis cases

Anchor piles are subjected to large concentrated forces due to wave/wind loading on the floating structure. Under strong earthquake shaking that could either lead to strain softening in clay or large excess pore pressure in sand, leading to liquefaction in extreme conditions, the holding capacity of the anchor might be reduced. In anchors with taut mooring, these conditions might even lead to the anchor pulling out of the soil. In the present study, the response of anchors with only catenary mooring, which is the most common type of anchoring, is studied. To this end, the soil model calibrated in the preceding sections was used. In a sensitivity analysis, the top layer was replaced with the loose Ottawa sand (i.e. same as the layer below). To assess the anchor response and effect of the anchor on the soil, the pore pressure buildup at points A to D in the soil at different depths (Fig. 9c) and the displacements of points 1 and 2 on top of the anchor pile (Fig. 9c) were computed for the various scenarios analyzed.

Possible different behavior of the soil inside the pile compared with

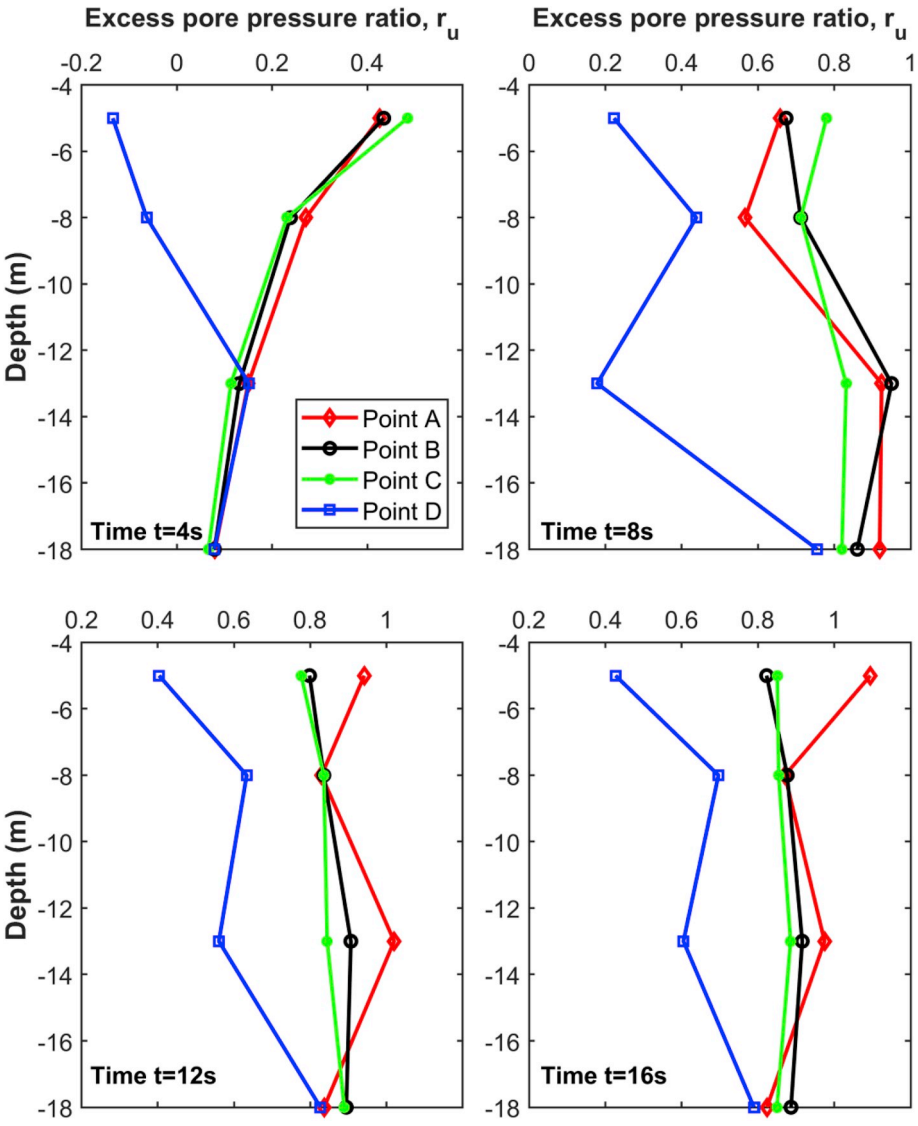

Fig. 17. Case 1 - Profiles of r_u with depth at monitoring points at four times.

the soil outside, might play a role on the response of the pile during liquefaction. For this reason, the monitoring point D was selected inside the pile to examine the confinement effect of the pile on liquefaction of the inner soil. The presence of the lid on top of the anchors, which is necessary in the case of suction anchors, may cause more confinement in the soil inside the pile. Therefore, the liquefaction triggering was assessed for anchors with and without a lid.

The following three analysis cases were considered in this study. In all cases, the static anchor load was assumed to be 50% of the ultimate lateral capacity of the anchor pile.

1) Profile with dense Monterey sand on the top and no anchor lid
2) Profile with loose Ottawa sand on the top and no anchor lid
3) Profile with loose Ottawa sand on the top and anchor with lid (suction anchor)

The analyses were speeded up by optimizing the model and mesh sizes through sensitivity studies. Increase of the pile thickness and use

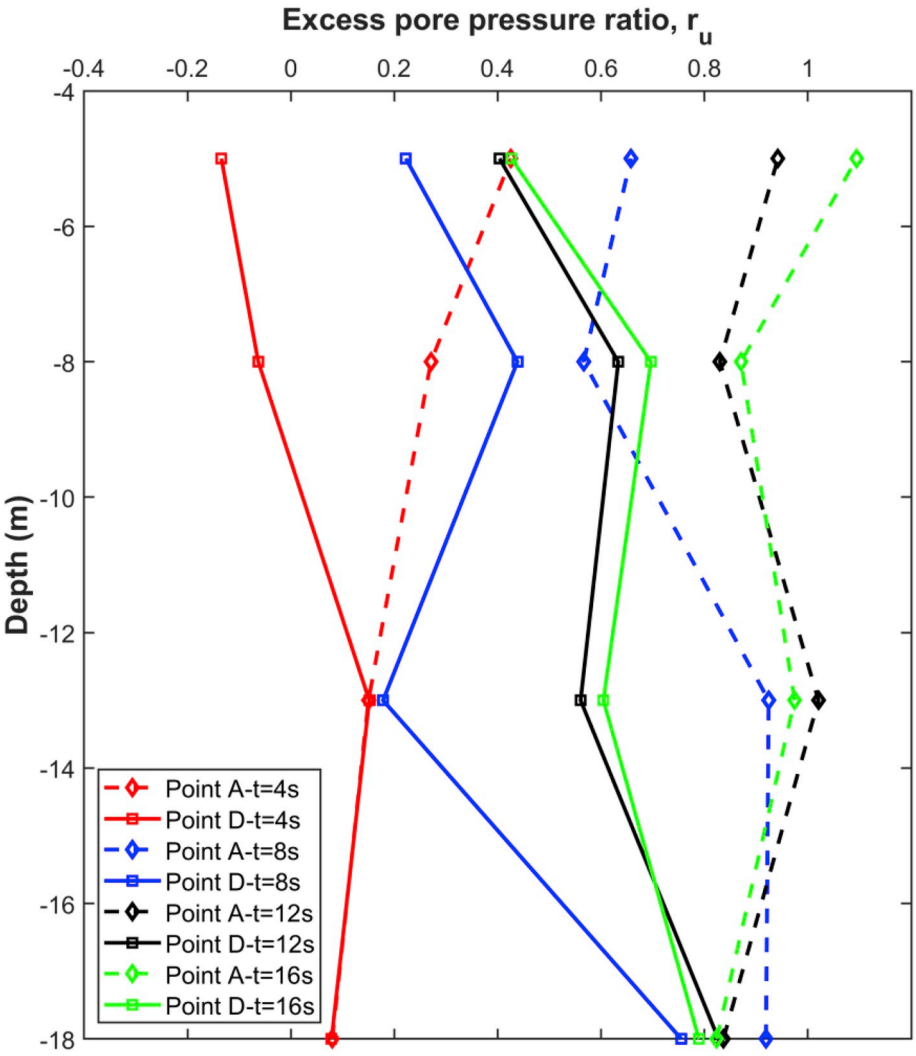

Fig. 18. Case 1 - Profiles of r_u with depth at monitoring points A and D at four times.

of small-strain solution, as described above, considerably reduced the calculation time. With these measures, each run took about 30 h using a PC with 3.5 GHz processor.

5. Results and discussions

Figs. 10–13 present the simulated excess pore water pressures at points A to D at different depths in Case 1 together with the corresponding values in the free field (i.e. no anchor present). As expected, the influence of the pile on the soil response diminishes with distance from the pile. On the other hand, as observed in Fig. 13, the pore pressure buildup inside the pile (point D) at all depths are lower than those in the free-field. This is believed to be due to the confinement by the anchor pile. This feature is more clearly observed in Fig. 14 which plots all the above results together for better comparison. The results show that in all cases, the excess pore pressure ratio, r_u, is less than 1.0. This parameters exceeds 1.0 only slightly at shallow depth (z = 2 m) at Point A which is closest to the anchor. The authors do not have an explanation for these values. They could be numerical artefacts due to the internal algorithm in FLAC3D for computation of the pore pressures. This feature is observed only at one point and during a short period of the response. Moreover, it does not have any negative effect on the stability of the results. Therefore, no attempt was made to study it in detail.

Fig. 15 illustrates the excess pore pressures at monitoring points A-D for Case 2 (considering the findings from Case 1, the pore pressures at point B can be taken as best representing the free field if a comparison with free field is of interest). A comparison between the excess pore pressures in Cases 1 and 2 reveals that replacing the top dense sand layer by the loose Ottawa sand does not significantly influence the

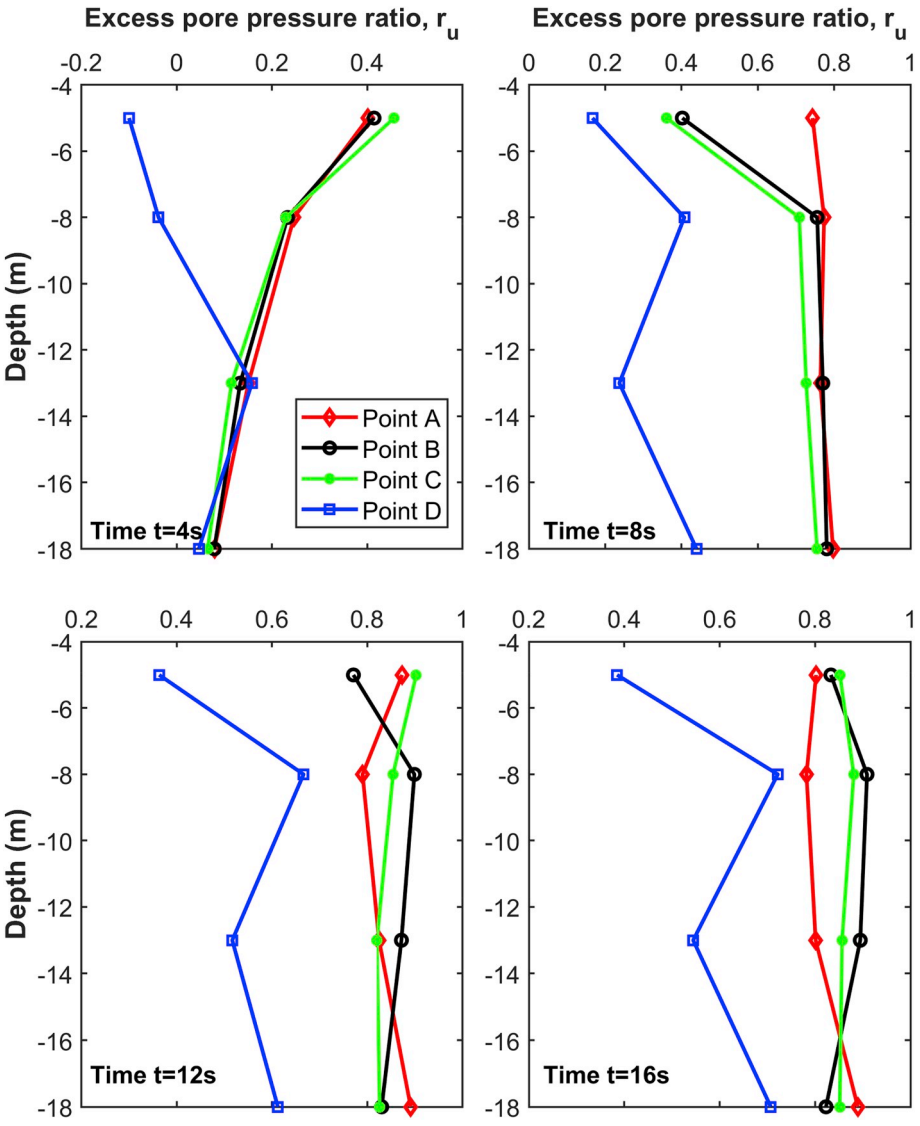

Fig. 19. Case 2 - Profiles of r_u with depth at monitoring points at four times.

excess pore pressures. As in Case 1, the pore pressures inside the anchor pile are lower than outside.

Fig. 16 displays the pore pressure buildup at monitoring points A-D for Case 3 (i.e. anchor pile with lid). Comparison of the excess pore pressures in this case with those in Case 2 indicates that the presence of the lid on top of the anchor does not affect the pore pressure generation significantly.

In order to gain insight into the progression of pore water pressure generation during the earthquake shaking, the variations of r_u with depth for Case 1 are plotted in Fig. 17 at four time instances 4, 8, 12 and 16 s. From this figure, it is easy to see that the pore pressure is always lower inside the anchor pile. For Points A and D, which are most affected by the presence of the anchor pile, Fig. 18 displays the profiles of excess pore water pressures at the same time instances. Figs. 19 and 20 present the same set of results for Case 2.

Fig. 21 depicts the displacement vectors in Case 1 at the end of earthquake shaking. It can be observed that the anchor tends to move laterally and rotate during the shaking.

Figs. 22–24 illustrate the lateral and vertical displacement time histories of points 1 and 2 on the anchor pile for the three cases considered. As shown in Fig. 22, the top of the pile (points 1 and 2) move horizontally about 55 cm during the shaking in Case 1. The negative

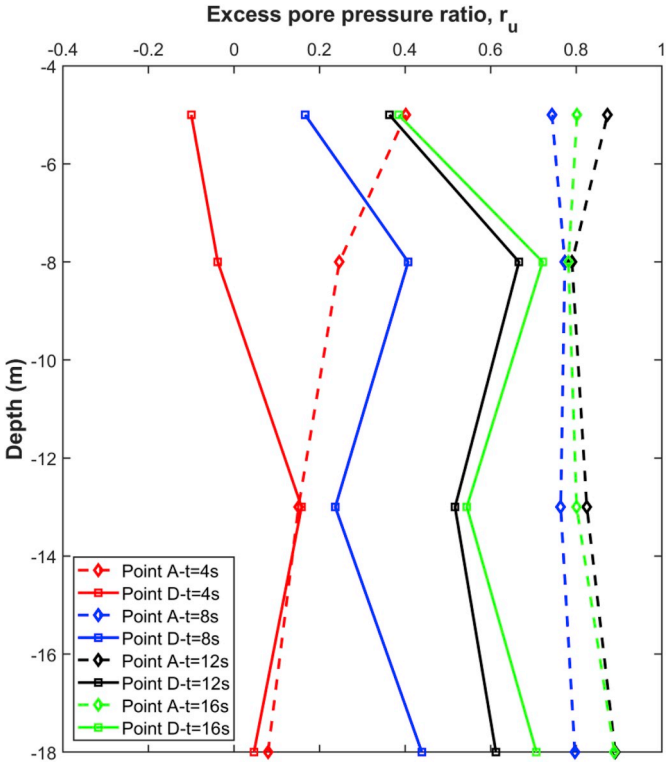

Fig. 20. Case 2 - Profiles of r_u with depth at monitoring points A and D at four times.

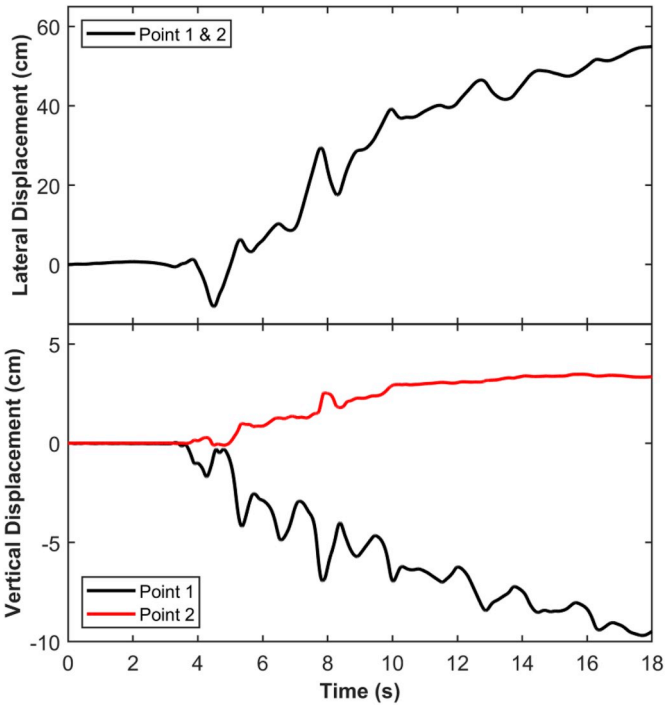

Fig. 22. Horizontal and vertical displacements of monitoring points on anchor pile in Case 1.

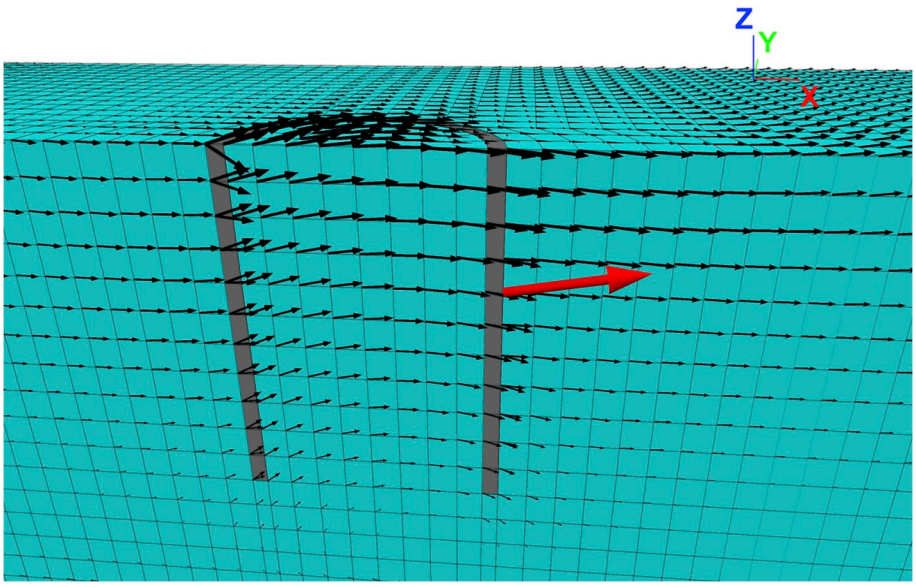

Fig. 21. Displacement vectors at end of dynamic analysis for Case 1.

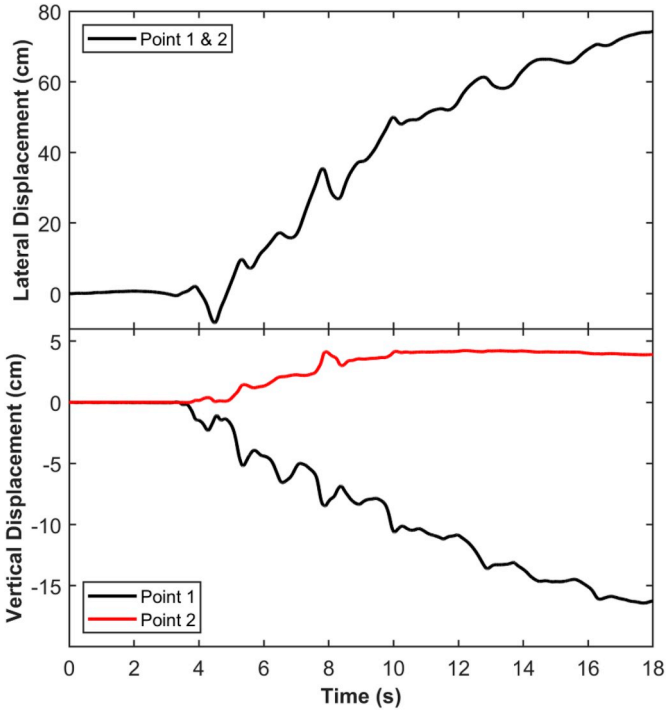

Fig. 23. Horizontal and vertical displacements of monitoring points on anchor pile in Case 2.

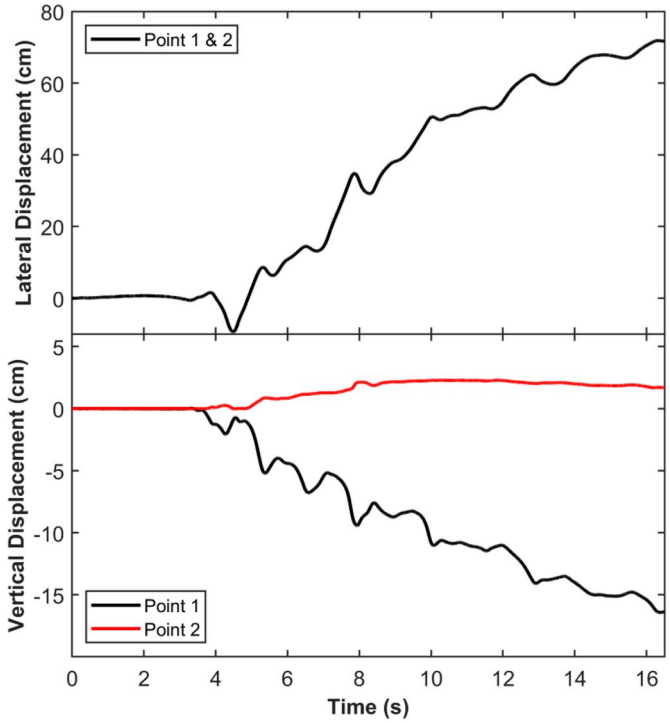

Fig. 24. Horizontal and vertical displacements of monitoring points on anchor pile in Case 3.

(downward) vertical displacements of point 1 (with permanent value of −10 cm) and the positive (downward) movement of the anchor at point 2 (with permanent value of 4 cm) indicate a combination of downward sinking and tilt of the anchor pile. These features sound logical.

The plots in Fig. 23 show that the horizontal permanent displacements at points 1 and 2 increase from 55 to 75 cm in Case 2 because of replacing the top layer with loose Ottawa sand. It also gives rise to an increase in the rotation of the pile (vertical displacement of point 1 from −10 to −16 cm and of point 2 from 4 to 5 cm). A comparison between the displacements in Case 2 and Case 3 (Fig. 24) indicates that the presence of the lid does not influence the displacements significantly. This is a very useful observation.

6. Concluding remarks

This paper has aimed at numerically investigating the effect of liquefaction on anchor piles for floating offshore structures and offshore wind turbines subjected to a combination of anchor load and earthquake shaking. To this end, three cases of soil-pile conditions were considered, and the pore pressure generation at the monitoring points in the soil at different depths and the displacements of the top of the anchor pile were computed.

The results have indicated that the excess pore pressures inside the pile are generally lower than those outside. Moreover, the presence of the lid on top of the pile does not influence the pore pressure buildup at the monitoring points. In other words, there is no significant differences in the behavior of geometrically identical anchor piles and suction anchors during liquefaction.

The horizontal displacements and rotations of the pile increase significantly when liquefaction extends to the surface. However, the results have shown that the presence of the lid does not significantly affect the displacements. In the cases considered, the permanent lateral displacements have been less than 80 cm. Such levels of displacements are generally not considered to pose any threat to the performance of the anchors. Anchors with small or no mooring loads are not expected to displace more than a few centimeters due to liquefaction. Analyses of a number of cases (not presented in the paper) have confirmed this.

Appendix A

A.1. Comparison of experimental and numerical results for monotonic drained triaxial tests for dense Ottawa sand

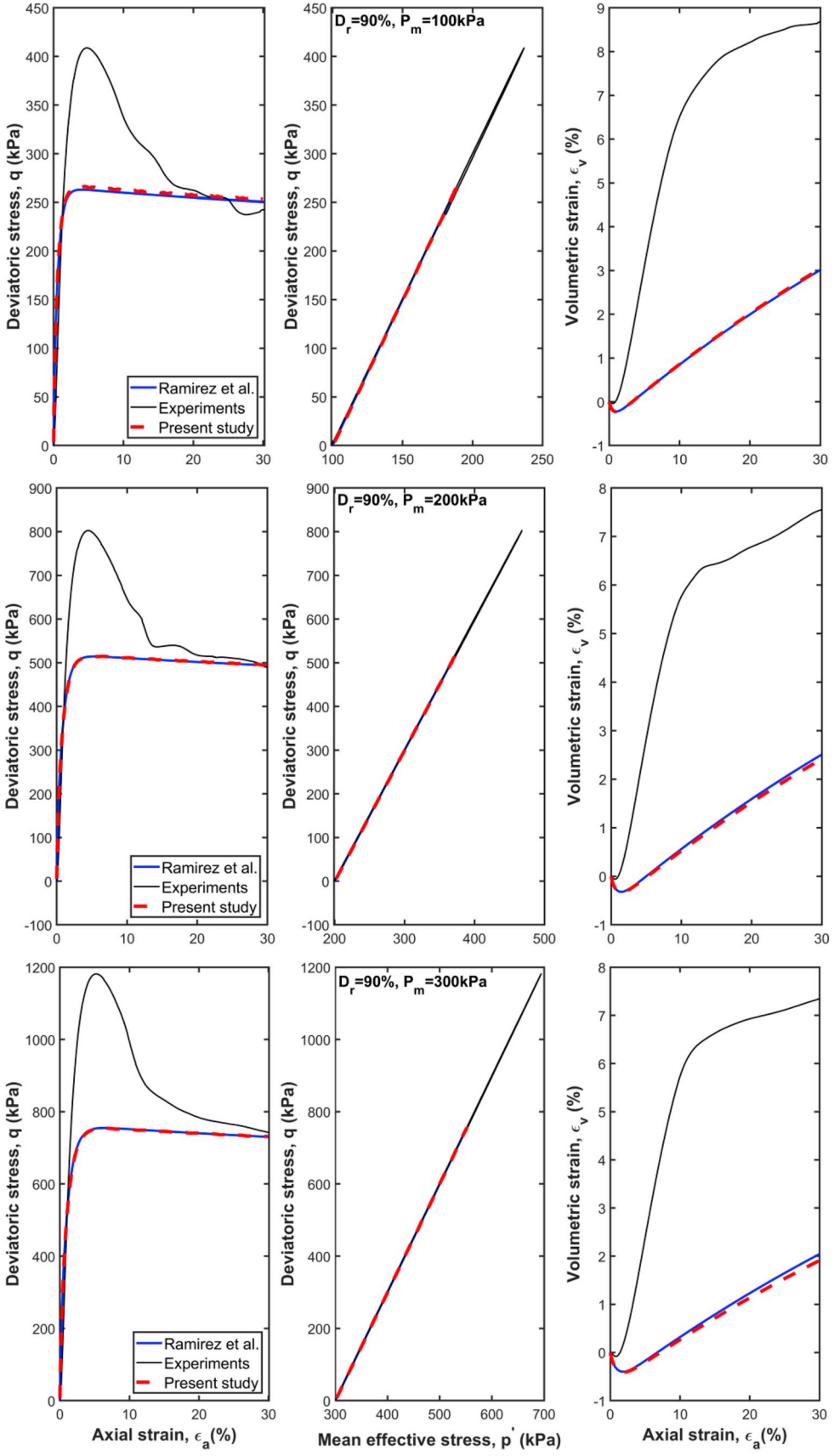

Fig. A.1. Comparison between numerical and experimental results for monotonic drained triaxial tests on dense Ottawa sand with $D_r = 90\%$

A.2. Comparison of experimental and numerical results for monotonic undrained triaxial tests on dense Ottawa sand

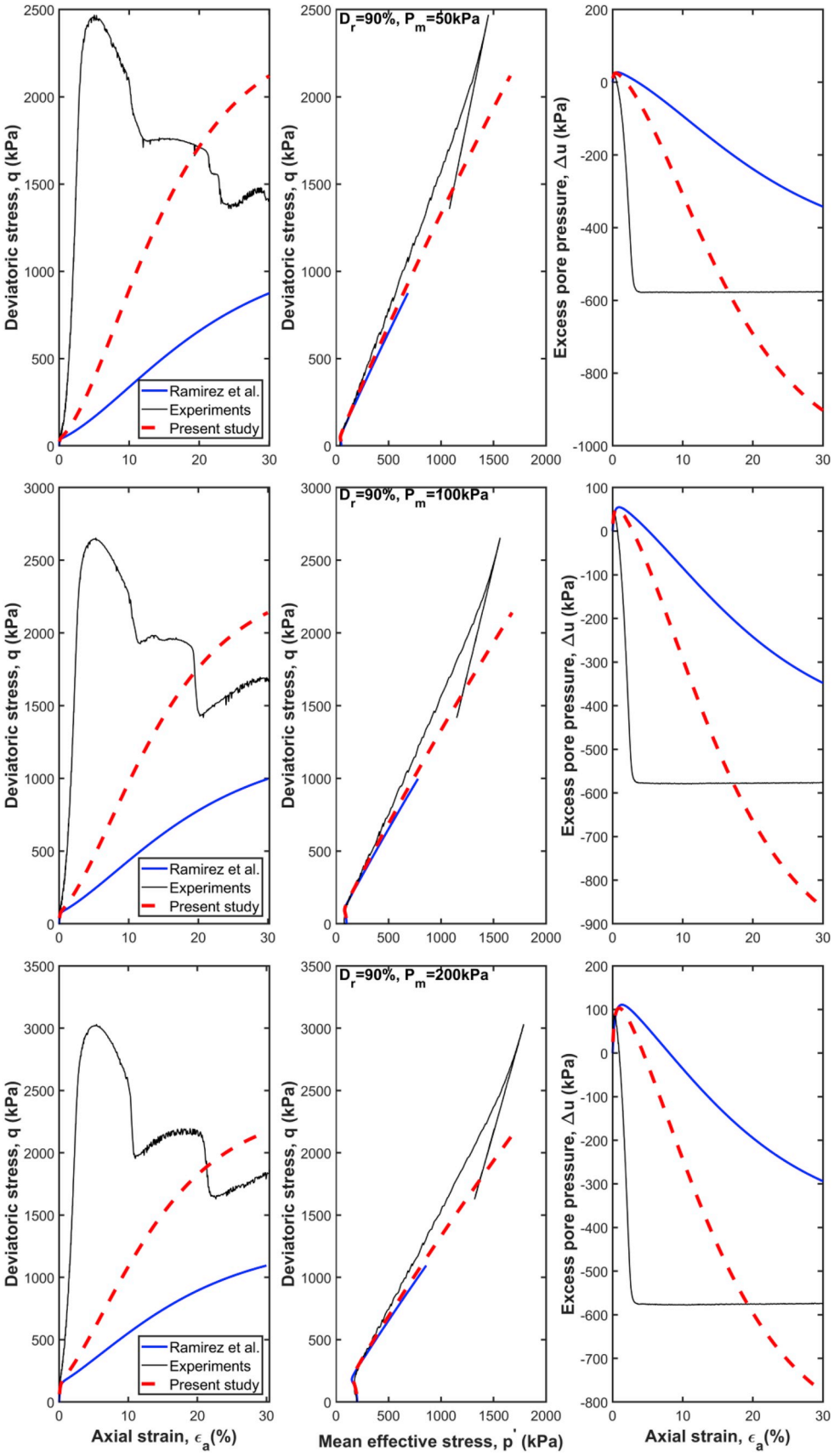

Fig. A.2. Comparison between numerical and experimental results for monotonic undrained triaxial tests on dense Ottawa sand with $D_r = 90\%$

A.3. Comparison of experimental and numerical results for cyclic undrained triaxial tests on Ottawa sand with $D_r = 60\%$

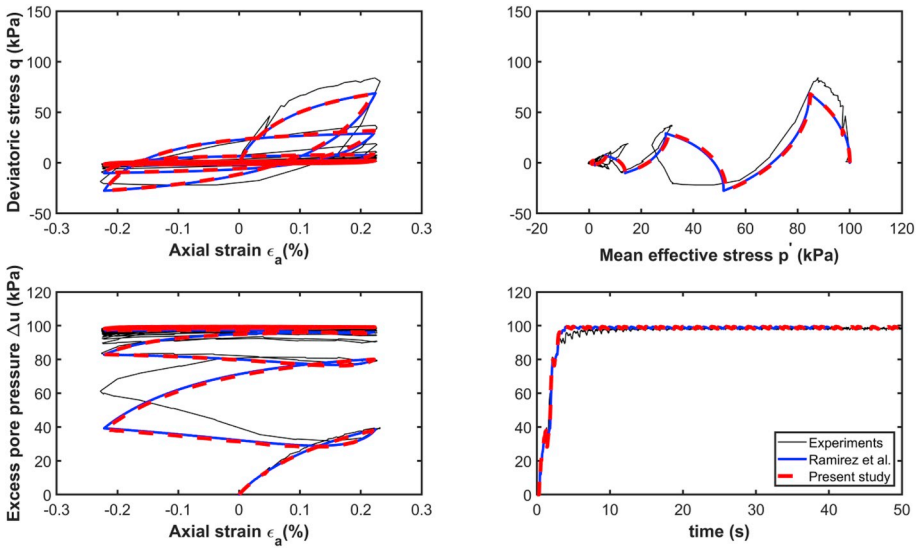

Fig. A.3. Comparison between numerical and experimental results for cyclic undrained triaxial tests on Ottawa sand with $D_r = 60\%$.

A.4. Comparison of experimental and numerical results for cyclic undrained triaxial tests on Ottawa sand with $D_r = 90\%$

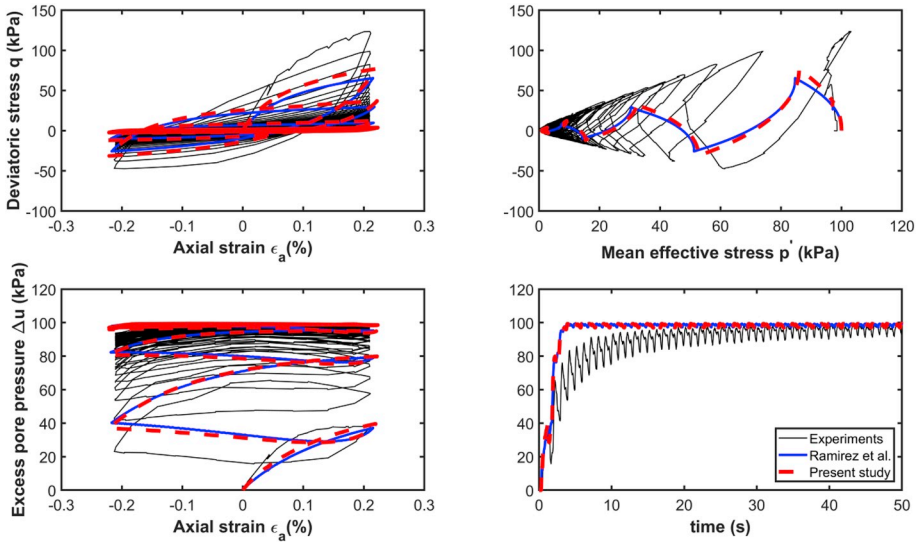

Fig. A.4. Comparison between numerical and experimental results for cyclic undrained triaxial tests on Ottawa sand with $D_r = 90\%$.

References

[1] WindEurope. Floating offshore wind energy: a policy blueprint for Europe. https://windeurope.org/policy/position-papers/floating-offshore-wind-energy-a-policy-blueprint-for-europe/.

[2] Kaynia AM. Seismic considerations in design of offshore wind turbines. Soil Dyn Earthq Eng 2018https://doi.org/10.1016/j.soildyn.2018.04.038.

[3] Asareh MA, Schonberg W, Volz J. Effects of seismic and aerodynamic load interaction on structural dynamic response of multi-megawatt utility scale horizontal axis wind turbines. Renew Energy 2016;86:49–58https://doi.org/10.1016/j.renene.2015.07.098.

[4] Smith V, Mahmoud H. Multihazard assessment of wind turbine towers under simultaneous application of wind, operation, and seismic loads. J Perform Constr Facil ASCE 2016;30(6):04016043https://doi.org/10.1061/(ASCE)CF.1943-5509.0000898.

[5] Kjørlaug RA, Kaynia AM, Elgamal A. Seismic response of wind turbines due to earthquake and wind loading. Proceedings of 9th international conference on structural dynamics, EURODYN 2014. Porto, Portugal. 2014.

[6] De Alba P, Seed HB, Chan CK. Sand liquefaction in large scale simple shear tests. J Geotech Eng Div ASCE 1976;102:909–27.

[7] Idriss IM, Boulanger RW. Soil liquefaction during earthquakes. Monograph MNO-12. Oakland, 10/02. Department of Civil and Environmental Engineering, University of California Davis, California, USA: Center for Geotechnical Modeling; 2010.

[8] Idriss IM, Boulanger RW. SPT-based liquefaction triggering procedures. Report UCD/CGM-10/02. Department of Civil and Environmental Engineering, University of California Davis, California, USA: Center for Geotechnical Modeling; 2010.

[9] Youd TL. Discussion of "examination and reevaluation of SPT-based liquefaction triggeringcase histories". J Geotech Geoenviron Eng ASCE 2013;139(11):1998–2000https://doi.org/10.1061/(ASCE)GT.1943-5606.0000876.

[10] Boulanger RW, Idriss IM. CPT-based liquefaction triggering procedure. J Geotech Geoenviron Eng ASCE 2015;142(2)https://doi.org/10.1061/(ASCE)GT.1943-5606.0001388.

[11] Lu CW. A simplified calculation method for liquefaction-induced settlement of shallow foundation. J Earthq Eng 2017;21(8):1385–405https://doi.org/10.1080/13632469.2016.1264327.

[12] Gobbi S, Lopez-Caballero F, Forcellini D. Numerical analysis of soil liquefaction induced failure of embankments. Proceedings of 6th ECCOMAS thematic conference on computational methods in structural dynamics and earthquake

engineering. Rhodes Island, Greece. 2017.
[13] Rapti I, Lopez-Caballero F, Modaressi-Farahmand-Razavi A, Foucault A, Voldoire F. Liquefaction analysis and damage evaluation of embankment-type structures. Acta Geotech. 2018;13(5):1041–59https://doi.org/10.1007/s11440-018-0631-z.
[14] Andrianopoulos KI, Papadimitriou AG, Bouckovalas GD. Bounding surface plasticitymodel for the seismic liquefaction nalysis of geostructures. Soil Dyn Earthq Eng 2010;30(10):895–911.
[15] Markou AA, Kaynia AM. Nonlinear soil-pile interaction for offshore wind turbines. Wind Energy 2018https://doi.org/10.1002/we.2178.
[16] Boulanger RW, Curras CJ, Kutter BL, Wilson DW, Abghari A. Seismic soil-pile-structure interaction experiments and analysis. J Geotech Geoenviron Eng ASCE 1999;125(9):750–9https://doi.org/10.1061/(asce)1090-0241(1999)125:9(750).
[17] Kourkoulis RS, Lekkakis PC, Gelagoti FM, Kaynia AM. Suction caisson foundationsfor offshore wind turbines subjected to wave and earthquake loading: effect of soil foundation interface. Geotechnique 2014;64(3):171–85https://doi.org/10.1680/geot.12.P.179.
[18] Kementzetzidis E, Corciulo S, Versteijlen WG, Pisanò F. Geotechnical aspects of offshore wind turbine dynamics from 3D non-linear soil-structure simulations. Soil Dyn Earthq Eng 2019;120:181–99https://doi.org/10.1016/j.soildyn.2019.01.037.
[19] Yang Z, Lu J, Elgamal A. OpenSees soil models and solid-fluid fully coupled elements: user's manual. California, USA: Departement of Structural Engineering, University of California San Diego; 2008.
[20] Dafalias YF, Manzari MT. Simple plasticity sand model accounting for fabric change effects. J Eng Mech 2004;130(6):622–34. 2004)130:6(622. https://doi.org/10.1061/(ASCE)0733-9399.
[21] Taiebat M, Jeremić B, Dafalias YF, Kaynia AM, Cheng Z. Propagation of seismic waves through liquefied Soils. Soil Dyn Earthq Eng 2010;30(4):236–57. April 2010.
[22] Boulanger RW, Ziotopoulou K. PM4Sand (Version 3): a sand plasticity model for earthquake engineering applications. Report UCD/CGM-15/01. University of California Davis, California, USA: Center for Geotechnical Modeling; 2015.
[23] Manzari MT, Arulanandan K. Numerical predictions for model no. 1. In: Arulanandan K, Scott RF, editors. Verification of numerical procedures for the analysis of soil liquefaction problems. Rotterdam, Netherlands: A.A. Balkema. 1993. p. 179–85.
[24] Ghofrani A, Arduino P. Prediction of LEAP centrifuge tests results using a pressure-dependent bounding surface constitutive model. Soil Dyn Earthq Eng 2018;113:758–70https://doi.org/10.1016/j.soildyn.2016.12.001.
[25] Ziotopoulou K. Seismic response of liquefiable sloping ground: class A and C numerical predictions of centrifuge model responses. Soil Dyn Earthq Eng 2018;113:744–57https://doi.org/10.1016/j.soildyn.2017.01.038.
[26] Ekstrom LT, Ziotopoulou K. Seismic response of liquefiable sloping ground: validation of class B predictions against the LEAP centrifuge tests. Geotechnical frontier 2017, Orlando, Florida. 2017https://doi.org/10.1061/9780784480489.034.
[27] Ramirez J, Barrero RA, Chen L, Dashti S, Ghofrani A, Taiebat M, Arduino P. Site response in a layered liquefiable deposit: evaluation of different numerical tools and methodologies with centrifuge experimental results. J Geotech Geoenviron ASCE 2018;144(10)https://doi.org/10.1061/(ASCE)GT.1943-5606.0001947.
[28] Kutter BL, Carey TJ, Hashimoto T, Manzari MT, Vasko A, Zeghal M, Armstrong RJ. LEAP database for verification, validation, and calibration of codes for simulation of liquefaction. 6th international conference on earthquake geotechnical engineering, Christchurch, New Zealand. 2015.
[29] Elgamal A, Yang Z, Parra E. Computational modeling of cyclic mobility and post-liquefaction site response. Soil Dyn Earthq Eng 2002;22(4):259–71https://doi.org/10.1016/S0267-7261(02)00022-2.
[30] Kirkwood P, Dashti S. A centrifuge study of seismic structure-soil-structure interaction on liquefiable ground and implications for design in dense urban areas. Earthq Spectra 2018;34(3):1113–34https://doi.org/10.1193/052417EQS095M.
[31] Biot MA. General theory of three-dimensional consolidation. J Appl Phys 1941;12(2):155–64https://doi.org/10.1063/1.1712886.
[32] Detournay E, Cheng AD. Fundamentals of poroelasticity. Fairhurst C, editor. Comprehensive rock engineering: principles, practice & projects, analysis and design methods, vol. 2. Oxford: Pergamon Press; 1993. p. 113–71.
[33] Manzari MT, Dafalias YF. A critical state two-surface plasticity model for sands. Geotechnique 1997;47(2):255–72https://doi.org/10.1680/geot.1997.47.2.255.